Research Article

Lubomír Lapčík*, Harun Sepetcioğlu, Yousef Murtaja, Barbora Lapčíková, Martin Vašina, Martin Ovsík, Michal Staněk, and Shweta Gautam

Study of mechanical properties of epoxy/graphene and epoxy/halloysite nanocomposites

https://doi.org/10.1515/ntrev-2022-0520
received October 3, 2022; accepted February 3, 2023

Abstract: This article aimed to compare various mechanical properties of epoxy/graphene and epoxy/halloysite nanocomposites. Graphene nanoplatelets (GnPs) and halloysite nanotubes (HNTs) were used as fillers at different concentrations. The studied fillers were dispersed in the epoxy resin matrices. Elastic–plastic mechanical behavior modulation was observed utilizing the fillers' nanoparticles and carboxyl-terminated butadiene–acrylonitrile copolymer rubber-modified epoxy resin. The hypothesis of the possible preceding inter-particle gliding of the individual GnPs in the complex resin nanocomposite matrix during mechanical testings was also confirmed. Increased ductility (elongation at break increased from 0.33 mm [neat matrix] to 0.46 mm [1 wt% GnPs] [39% increase]) and plasticity of the GnP nanocomposite samples were observed. In contrast, the decreasing mechanical stiffness as reflected in the decreased Young's modulus of elasticity (from 3.4 to 2.7 GPa [20% decrease]) was found for the epoxy/HNT nanocomposites. The obtained dynamic stiffness of the investigated nanocomposites confirmed the complexity of the mechanical response of the studied material systems as a combination of the ductile and brittle phenomena.

Keywords: graphene, halloysite, nanocomposites, epoxy polymer, CTBN rubber, mechanical testing

1 Introduction

Polymeric and resin-based nanocomposites are widely used in material engineering research owing to their capacity to modulate plastic–elastic mechanical performance at static and dynamic mechanical loadings [1]. These nanocomposites are characterized by high mechanical toughness and wear resistance, improved self-lubrication properties, and low friction coefficient [2,3]. Therefore, they have a wide range of application potential in the aerospace [4], automotive [5], chemical, and electronic industries as well as high-voltage outdoor insulation materials [6–8].

The ability of a material to absorb mechanical impact, *i.e.*, its toughness, requires high force resistance and the existence of the deformation mechanisms that absorb and dissipate the applied mechanical energy over a large path, in a large volume, and for a sufficiently long time. Such mechanisms may be inherent in the material due to its specific microstructure but can also be deliberately incorporated into the structure of polymer/epoxy resin composites and blends [9,10]. Such synergistic effect can be obtained by proper selection of the combination of the nanofiller particles' type (graphene nanoplatelets [GnPs], halloysite nanotubes [HNTs], *etc.*), shape, and surface chemistry, by modulating the physicochemical characteristics of the matrix, *etc.*, for example, by adding rubbery plastic components [11,12]. However, literature indicates that relatively few studies have focused on carboxyl-terminated butadiene–acrylonitrile (CTBN) copolymer rubber-modified epoxy

* **Corresponding author: Lubomír Lapčík,** Department of Physical Chemistry, Faculty of Science, Palacky University, 17. Listopadu 12, 771 46 Olomouc, Czech Republic; Faculty of Technology, Tomas Bata University in Zlin, Nam. T.G. Masaryka 275, 760 01 Zlin, Czech Republic, e-mail: lapcikl@seznam.cz
Harun Sepetcioğlu: Department of Metallurgy and Mechanical Engineering, Technology Faculty, Selçuk University, Konya 42075, Turkey
Yousef Murtaja: Department of Physical Chemistry, Faculty of Science, Palacky University, 17. Listopadu 12, 771 46 Olomouc, Czech Republic
Barbora Lapčíková: Department of Physical Chemistry, Faculty of Science, Palacky University, 17. Listopadu 12, 771 46 Olomouc, Czech Republic; Faculty of Technology, Tomas Bata University in Zlin, Nam. T.G. Masaryka 275, 760 01 Zlin, Czech Republic
Martin Vašina: Faculty of Technology, Tomas Bata University in Zlin, Nam. T.G. Masaryka 275, 760 01 Zlin, Czech Republic; Department of Hydromechanics and Hydraulic Equipment, Faculty of Mechanical Engineering, VŠB-Technical University of Ostrava, 17. Listopadu 15/2172, 708 33 Ostrava-Poruba, Czech Republic
Martin Ovsík, Michal Staněk, Shweta Gautam: Faculty of Technology, Tomas Bata University in Zlin, Nam. T.G. Masaryka 275, 760 01 Zlin, Czech Republic

resins filled with GnPs exhibiting the improved fracture toughness [13–16].

Several polymer composites have been reported in recent years, including polyester, polyurethane, epoxy, and phenolics [17,18]. Among these, epoxy polymer composites have gained tremendous attention due to their high mechanical toughness and moisture absorption properties [19]. Additionally, these resins show less shrinkage and less toxic emissions during the curing process [20]. Therefore, epoxy resins are considered high-quality materials on an industrial scale, despite their high cost [21].

In general, the plastic or viscoelastic deformation of materials in front of the crack apex removes part of the crack energy and thus controls its progress within the matrix. Therefore, the difference between brittle and ductile fractures is in their spatial localization and their temporal progression. Most polymer composite materials can break down by either brittle or ductile fractures depending on the external conditions or processes taking place in the material. The transition between ductile and brittle fractures can be temperature dependent, with the temperature regions of the two distinct mechanisms separated by the embrittlement temperature. The latter always lies below the glass-transition temperature. In the same sense, with a drop in temperature, an increase in loading rate can have an effect – although the difference in loading rate must be an order of magnitude greater to have an effect on the nature of the fracture. However, long-term static loading below the yield stress for many polymers also leads to brittle fracture. In this case, the "material self-defence" mechanisms cannot develop sufficiently by creating a plastic zone in front of the crack tip [9].

Tribological properties of resins often indirectly influence their mechanical strength, whereas epoxy resins exhibit limited tribological properties [22]. For example, the service life of pipes made of polymeric composites depends on the effectivity of the energy dissipation during fluid flow, the character of which is dependent on the wall friction of the transported medium. Such pipes are exposed under service conditions to long-term stresses, usually under relatively low temperatures, but sometimes also at the interaction of an active environment. Under these conditions, they cannot properly develop the "self-defense" mechanisms of crack blunting by local plastic deformation, and from the exposed surface small cracks propagate inside the material or even sharp cracks, which eventually lead to brittle fracture [9].

Several methods have been reported to improve these properties, *i.e.*, adding micro- and nano-sized particles as fillers in the resin matrix [23,24]. A large variety of nanofillers, such as SiO_2, MnO_2, TiO_2, Al_2O_3, SiC, Si_3N_4, ZnO, MoS_2, nanoclay, and carbon nanotubes, have been reported in different types of polymeric resins [25–28]. These fillers have demonstrated varying efficiencies with certain limitations, which hinder their practical applications [29].

GnPs, consisting of 30–40 layers of graphene, are widely used nanomaterials due to their high thermal stability and conductivity, high Young's modulus of elasticity, high optical transmittance, high fracture strength, and improved lubrication properties [17,30]. Due to their inherent, intrinsic energy-dissipating mechanisms (sheet bending and sliding), GnPs belong to highly advanced materials used in composite manufacturing [17,31]. However, it is necessary to optimize the content of graphene nanofillers in epoxy resins because higher content leads to nonuniform distribution of graphene in the polymer network [32]. Another challenge is the observed high aggregation rates of graphene arising from the acting Van der Waals interaction forces [33–35]. For this reason, it is necessary to optimize a proper mass ratio of graphene nanofillers to epoxy resin in order to obtain the desired mechanical properties.

Halloysite, an aluminosilicate clay material [36], is another filler commonly used in polymer resins owing to its cylindrical structure, improved mechanical performance, and low cost [37,38]. HNTs exhibit higher dispersion ratio and have surface hydroxyl groups with low density, which results in their smooth diffusion into the polymer matrix, leading to less aggregation [39]. Moreover, due to small basal spacing of crystal planes, the intercalation of HNTs with polymers and additives is difficult [40,41]. However, HNT nanofillers belong to potential functional fillers used in industrial practice [42,43].

Published results confirmed synergistic combination of the plastification effect of the rigid epoxy matrix assigned to the gliding of the individual GnP nanofillers and the stiffening effect of the HNT nanofillers when fracture toughness increased. The latter plastification was also enhanced by the addition of the CTBN polymeric rubber component of the composite epoxy matrix, thus improving material's fracture toughness. A similar effect was also confirmed by molecular dynamics simulations of mono helical soft segments based on Newtonian mechanics theory [44].

In this study, GnPs and HNTs were used separately as fillers to improve the mechanical performance, dispersion, thermal stability, and opto-electronic properties of the epoxy resin composite. A varying mass ratio of both fillers was used in prepared composites, and the effect of the applied nanofillers was evaluated by uniaxial tensile testing, fracture toughness measurements, uniaxial bending testing, indentation micro-hardness measurements, and nondestructive vibration testing.

2 Materials

2.1 Materials

The resin and hardener used in this study were diglycidyl ether of bisphenol A resin (DGEBA) with low viscosity (trade name: laminating resin MGS L285) (Figure 1a) and 3-aminomethyl-3,5,5 trimethylcyclohexylamine (trade name: L285), respectively (both materials were provided from Hexion, USA) (Figure 1b). The liquid rubber used was CTBN copolymer (purchased from Zibo Qilong, China) with an average of 0.58–0.65 carboxyl groups per molecule; its number average molecular weight was about 3,800 Da, and the content of acrylonitrile was of 8–12% (Figure 1c). The technical data of the CTBN are given in Table 1. The chemical structures of epoxy, hardener, and CTBN are shown in Figure 1. Nanofillers used in this study were non-functionalized planar-shaped GnPs of 800 m^2/g specific surface area, layer thickness of 3–7 nm with an average layer width of 1.5 µm, and 99.9% purity (purchased from Nanografi, Ankara, Turkey). The HNTs ($Al_2Si_2O_5(OH)_4$) used had two layers of nanocylindrical structure (Esan Eczacıbası (Istanbul, Turkey)), whose inner diameter, outer diameter, and length were in the range of 1–20, 30–50, and 100–800 nm, respectively.

2.2 Preparation of nanocomposites and epoxy blends

2.2.1 CTBN–epoxy blends

The chemical formulas of the used epoxy blends are shown in Figure 1. For preparing the epoxy blends with CTBN liquid rubber, 10 wt% CTBN was mechanically

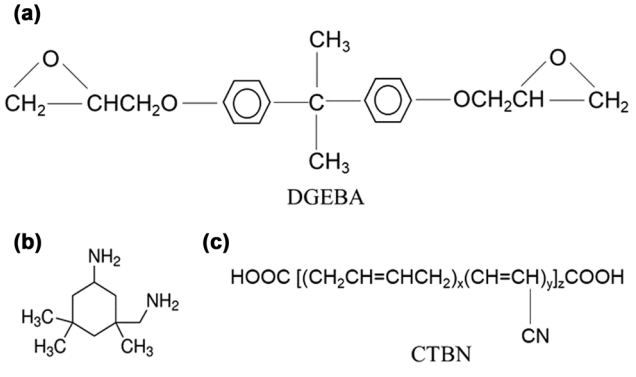

Figure 1: The chemical structure of components (a) DGEBA, (b) 3-aminomethyl-3,5,5-trimethylcyclohexylamine, and (c) CTBN.

Table 1: Properties of the applied CTBN liquid rubber

Parameter	Value
Viscosity (40°C) (Pa s)	7–12
Carboxyl content (mmol/g)	0.58–0.65
Nitrile group content (%)	8.0–12.0
Water content (%)	≤0.05
Volatile content (%)	≤2.0

mixed with epoxy resin in a glass beaker placed on a preheated plate. The blends in the beaker were then stirred by ultrasonication for 15–20 min to obtain homogeneous blends, followed by 1 h of degassing in the vacuum oven at 60°C. The amine-based curing agent was subsequently added at a stoichiometric ratio of 80:20 (epoxy:hardener) by weight at slow stirring. Blends were subsequently cast into molds and cured for 1 h at 90°C, followed by 3 h post-curing at 120°C.

2.2.2 CTBN– GnPs–epoxy and CTBN–halloysite–epoxy composites

The nano-reinforcement ratios of the epoxy mixtures were created based on the literature. Many authors [43,45–49] have experimentally studied the concentration of GnP and HNTs in the epoxy matrix to be in the range of (0–1) and (0–5) wt%, respectively, and reported the effect of these concentrations on tensile, fracture, and flexural properties of the neat matrix. For preparing the epoxy mixtures with GnPs and HNTs (see Figure 2 for scanning electron microscopy [SEM]), 0, 0.125, 0.25, 0.5, 0.75, and 1 wt% GnPs and 0, 1, 2, 3, 4, and 5 wt% HNTs were added to the epoxy resin, and the obtained mixtures were transferred into a RETSCH-PM 100 planetary mill for mixing at a rotation rate of 200 rpm for 25 h. The epoxy composite mixtures were prepared using 10 mm diameter balls and a bowl made of tungsten carbide as mixing media. The mixing bowls were loaded with the epoxy mixtures and balls, resulting in a ball-to-powder mass ratio of 30:1. First, the mixtures were mixed for 30 min, then rested for 10 min to avoid overheating, then mixed again, and the cycle was continued until the decided mixing time was completed. Subsequently, 10 wt% CTBN was added to each epoxy mixture containing the GnP and HNT reinforcements for preparing the CTBN–GnPs–epoxy and CTBN–HNTs–epoxy composites. The prepared mixtures were stirred using ultrasonication for 25–30 min to obtain the homogeneous mixtures, followed by degassing in a vacuum oven at 60°C for about 1 h. Finally, the curing procedure of CTBN–epoxy blends

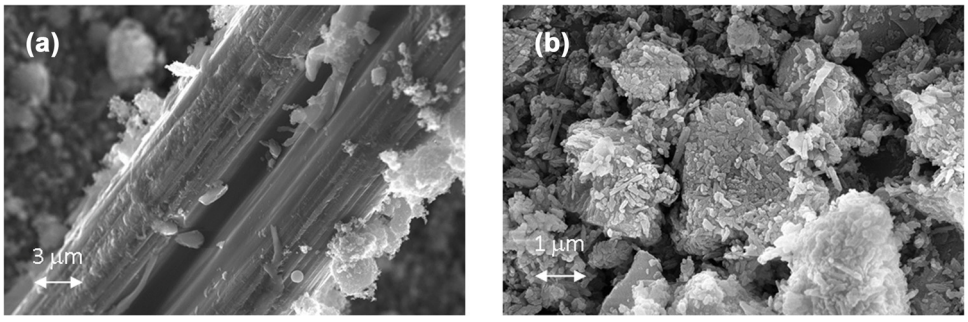

Figure 2: SEM images of the studied fillers: (a) GnPs, (b) HNT.

described in Section 2.2.1 was followed to cure the CTBN–GnPs–epoxy and the CTBN–HNTs–epoxy composites. The same CTBN liquid rubber concentration of 10 wt% was used in all of the investigated epoxy/graphene and epoxy/halloysite nanocomposites; the virgin epoxy matrix prepared was without CTBN liquid rubber.

3 Methods

3.1 SEM analysis

Zeiss EvoLS10 equipped with an energy-dispersive X-ray detector (Germany) was used for SEM analysis. SEM images were taken by depositing nanofiller samples on a standard 400-grid copper mesh. Fillers' acetone dispersions were ultrasonicated for 15 min, cast on the copper mesh, and air dried. SEM measurements were performed at an accelerating voltage of 2 kV.

3.2 Uniaxial tensile testing

Universal Testing Machine Autograph AGS-100 Shimadzu (Japan) and Zwick 1456 multipurpose tester (Zwick Roell, Ulm, Germany) equipped with Compact Thermostatic Chamber TCE Series were used for tensile testing of injection-molded specimens. All data were recorded as per ČSN EN ISO 527-1 and ČSN EN ISO 527-2 standards for the tested gauge length of 80 mm. All experiments were performed at room temperature up to break with a 50 mm/min deformation rate. Young's modulus of elasticity and elongation at break were obtained from the stress–strain dependency plots. Each experiment was repeated 10×, and mean values and standard deviations of the measured quantities were subsequently calculated. All experiments were performed at the ambient laboratory temperature of 25°C.

3.3 Charpy impact testing

Impact tests were carried out using Zwick 513 Pendulum Impact Tester (Zwick Roell, Ulm, Germany) according to the ČSN EN ISO 179-2 standard, allowing a 25 J energy drop. Each experiment was repeated 10× and mean values and standard deviations of the fracture toughness were calculated. All experiments were performed at the ambient laboratory temperature of 25°C.

3.4 Micro-hardness

Micro-indentation tests were performed on a micro-indentation tester (Micro Combi Tester, Anton Paar, Austria), according to the ČSN EN ISO 14577 standard. The applied diamond tip was cube-corner shaped (Vickers, Anton Paar, Austria). Measurement parameters were set as follows: the maximum load of 3 N, loading rate (unloading rate) of 6 N/min, and holding time of 90 s. All experiments were performed according to the depth-sensing indentation method, allowing simultaneous measurement of the acting force on the indenter and the displacement of the indenter's tip. The indentation modulus (E_{IT}) was calculated from the plane strain modulus of elasticity (E^*) using an estimated Poisson's ratio (ν) of the samples (0.3–0.4 [50,51]):

$$E_{IT} = E^*(1 - \nu^2). \quad (1)$$

Each measurement was repeated 10×, and mean values and standard deviations of the indentation modulus were calculated. All experiments were performed at the ambient laboratory temperature of 25°C.

3.5 Uniaxial three-point bending tests

The uniaxial three-point bending test was carried out on a Zwick 1456 testing machine (Zwick Roell GmbH &Co. KG, Ulm, Germany) according to the ČSN EN ISO 14125 standard. The results were evaluated using the TestXpert software. The distance between the supports was set to 64 mm, and the roundness of the supports and the load mandrel was 5 mm. The deformation rate during the three-point bending test was 1 mm/min, and the loading velocity was 50 mm/min.

3.6 Displacement transmissibility measurements

Displacement transmissibility T_d is expressed by the following equation [52]:

$$T_d = \frac{y_2}{y_1} = \frac{a_2}{a_1}, \tag{2}$$

where y_1 is the displacement amplitude on the input side of the tested sample, y_2 is the displacement amplitude on the output side of the tested sample, a_1 is the acceleration amplitude on the input side of the tested sample, and a_2 is the acceleration amplitude on the output side of the tested sample. The displacement transmissibility of a spring–mass–damper system, which is described by spring (stiffness k), damper (damping coefficient c), and mass m, is given by the following equation [53]:

$$T_d = \sqrt{\frac{k^2 + (c \bullet \omega)^2}{(k - m \bullet \omega^2)^2 + (c \bullet \omega)^2}} = \sqrt{\frac{1 + (2 \bullet \zeta \bullet r)^2}{(1 - r^2)^2 + (2 \bullet \zeta \bullet r)^2}}. \tag{3}$$

Under the condition $dT_d/dr = 0$ in equation (3), it is possible to obtain the frequency ratio r_0 at which the displacement transmissibility reaches its maximum value [54,55]:

$$r_0 = \frac{\sqrt{\sqrt{1 + 8 \bullet \zeta^2} - 1}}{2 \bullet \zeta}. \tag{4}$$

It is evident from equation (4) that the local extreme of the displacement transmissibility is generally shifted to lower values of the frequency ratio r with increasing damping ratio ζ (or with decreasing material mechanical stiffness k). The local extrema (*i.e.*, the maximum value of the displacement transmissibility T_{dmax}) is found at the frequency ratio r_0 from equation (4). The mechanical vibration tests were performed by forced oscillation method. The displacement transmissibility T_d was experimentally measured using the BK 4810 vibrator in combination with a BK 3560-B-030 signal pulse multi-analyzer and a BK 2706 power amplifier at the frequency range from 2 to 3,200 Hz. The acceleration amplitudes a_1 and a_2 on the input and output sides of the investigated samples were recorded by BK 4393 accelerometers (Brüel & Kjær, Nærum, Denmark). Measurements of the displacement transmissibility were done for three different inertial masses m (for 0, 90, and 500 g), which were placed on the top side of the tested samples. The dimensions of the tested specimen were 60 mm × 60 mm × 3 mm (length × width × thickness). Each measurement was repeated 5× at an ambient temperature of 22°C.

4 Results and discussion

A typical shape of the used nanofillers, as observed by SEM analysis, is shown in Figure 2. Here the GnP lamellar structure was clearly visible in Figure 2a with a layer thickness of about 3–7 nm and an average layer width of 1.5–2.0 µm. In contrast, the HNT nanotubes exhibited a compact coagulated structure composed of individual nanotubes of approximately 30–50 nm diameter and 100–800 nm length (Figure 2b).

Results of the tensile-testing experiments of the studied nanocomposites are shown in Figure 3. There was a decrease of the Young's modulus of elasticity (E) during uniaxial testing from 3.4 GPa (neat matrix) to 2.7 GPa (for 1 wt% epoxy/GnP nanocomposite) with increasing GnP filler concentration [56]. This effect was accompanied by the increasing nonlinear trend of the obtained magnitudes of the elongation at break, indicating increasing ductility and plasticizing effect of the GnP nanofiller on the mechanical behavior of the prepared epoxy/GnP nanocomposites. Based on the literature [11], it was assumed that this behavior was ascribed to the gliding of the individual nanoplatelet sheets within complex epoxy/GnP nanocomposite matrix accompanied by the crack deflection, layer breakage, and separation/delamination of GnP layers [13]. However, the opposite effect was found in the case of the epoxy/HNT nanocomposites, where the E decreased from 3.4 GPa (neat matrix) to 2.7 GPa (for 5 wt% epoxy/HNT nanocomposite), thus indicating the decreasing mechanical stiffness of the studied materials. Simultaneously, in contrast to the epoxy/GnP nanocomposites, a more brittle behavior with increasing HNT filler concentration was observed. These observations were demonstrated by constant elongation at break (about 0.36 mm) dependency as shown in Figure 3.

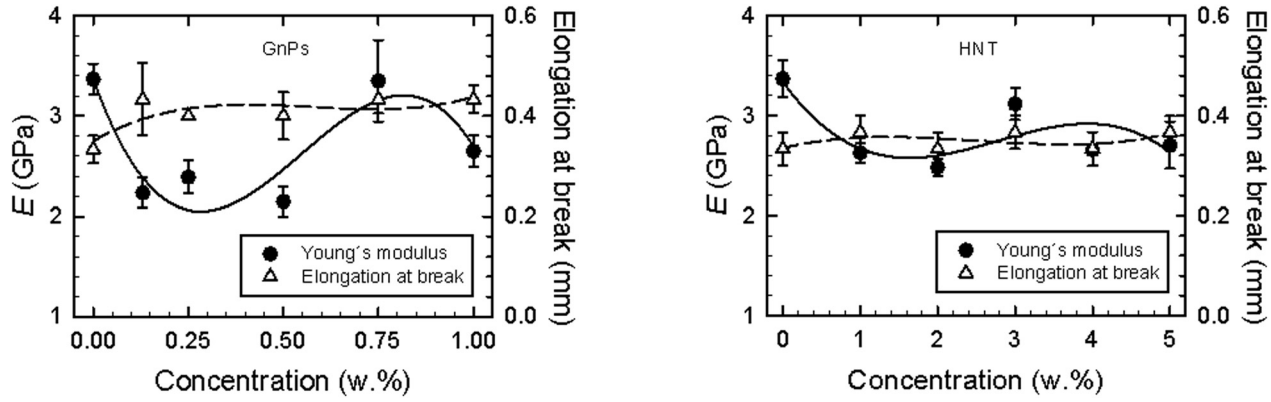

Figure 3: Nanofiller concentration dependencies of the Young's modulus of elasticity and the elongation at break of the studied GnPs and HNT nanocomposites. Applied deformation rate was of 50 mm/min. Continuous line – Young's modulus of elasticity, dashed line – elongation at break.

Based on the aforementioned facts, it was assumed that the HNT nanofiller increased the brittleness of the composite due to the limited movement of the stiffened HNT nanotubes resulting in the hindered gliding of the HNT nanofillers within the composite matrix.

The above-mentioned results of the uniaxial tensile tests were in excellent agreement with the observed fracture toughness measurements (Figure 4), where higher fracture toughness of 8.2 kJ/m^2 of epoxy/HNT nanocomposites was found compared to the 6.0 kJ/m^2 of epoxy/GnP nanocomposites (both at 1 wt% filler concentration). At higher HNT filler concentrations (in the concentration range of 1–5 w%) nonlinear decreasing trend of fracture toughness was observed (Figure 4).

In addition, the presence of CTBN (Figure 1c) acted on the continuous composite matrix as a kind of accelerator, which forces it to develop local deformations. The deformation mechanisms in the matrix then dissipate the external mechanical energy over a large volume, thus preventing the development of a single brittle crack. Optimal performance of rubber modification requires several conditions to be met, namely the establishment of a two-phase morphology, the provision of satisfactory interfacial adhesion, and the establishment of a certain critical distance between adjacent rubber domains [9]. Analogous behavior was observed for multi-phase hard and soft segmental flexible polymers, where hard phases served as stiffening element and the soft phases provided elasticity [44].

Results of the micro-hardness *vs* filler concentration measurements of both the studied epoxy nanocomposites are shown in Figure 5. A nonlinear decreasing trend of the indentation modulus E_{IT} with increasing filler concentration was observed. In the case of the epoxy/GnP nanocomposites, E_{IT} decreased from 4.3 GPa (neat matrix) to 3.4 GPa (for 1 wt% GnP nanocomposite). Similarly, in the case of the epoxy/HNT nanocomposites, E_{IT} decreased from 4.3 GPa (neat matrix) to 3.8 GPa (for 5 wt% HNT

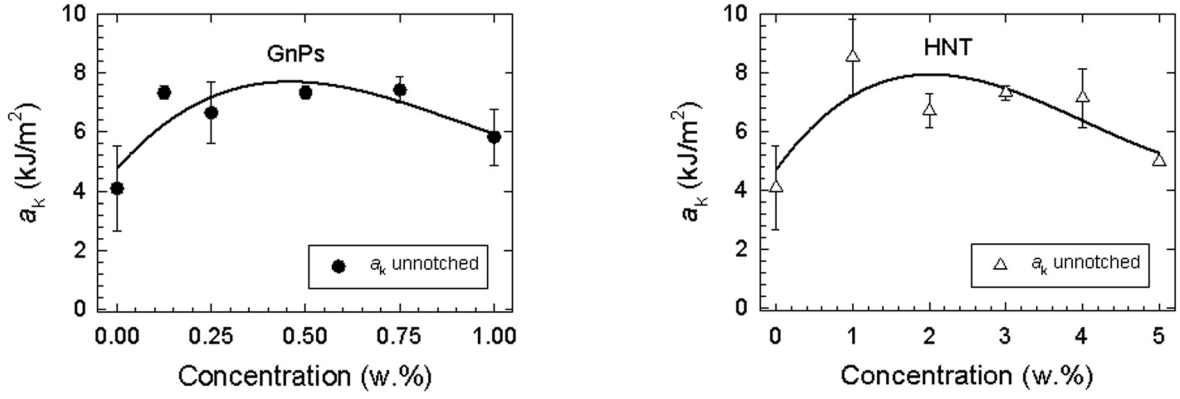

Figure 4: Nanofiller concentration dependencies of the unnotched fracture toughness of the studied GnPs and HNT nanocomposites.

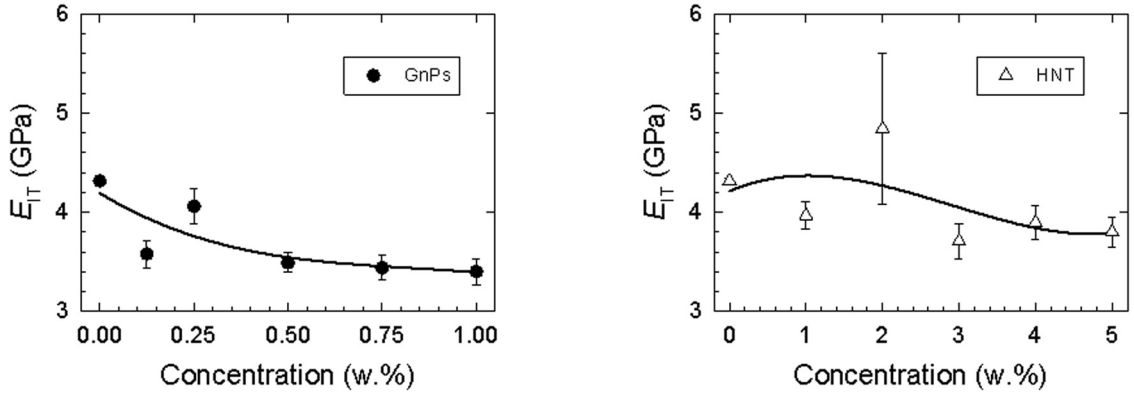

Figure 5: Nanofiller concentration dependencies of the indentation modulus of the studied GnPs and HNT nanocomposites.

nanocomposite). The plasticizing effect of the applied nanofillers was assumed as the most probable cause of this decrease of surface hardness.

Results of the uniaxial three-point bending tests of the studied nanocomposites are shown in Figure 6. Here, nonlinear decreasing patterns were found for both the studied nanocomposites. Such behavior is typical for brittle materials. A nonlinear decrease of the bending modulus (E_B) from 4.3 GPa (neat matrix) to 2.8 GPa (for 1 wt% GnP nanocomposite) with increasing GnP filler concentration was found. This effect was accompanied by the increasing gradual nonlinear trend of the obtained magnitudes of the elongation at break (from 5.0 mm [neat matrix]) to 6.0 mm (for 1 wt% epoxy/GnP nanocomposite), indicating increasing composite ductility due to the plasticizing effect of the nanofiller of the prepared epoxy/GnP nanocomposites. In the case of the epoxy/HNT nanocomposites, E_B nonlinearly decreased from 4.3 GPa (neat matrix) to 3.0 GPa (for 5 wt% epoxy/HNT nanocomposites), indicating decreasing mechanical stiffness of the studied materials. However, the opposite, a minor decreasing nonlinear trend of the elongation at break *vs* HNT filler concentration, was found, where the elongation at break decreased from 5.0 mm (neat matrix) to 4.1 mm (for 5 wt% epoxy/HNT nanocomposites). These results indicated higher brittleness of the epoxy/HNT nanocomposites compared to the epoxy/GnP nanocomposites.

Results of the dynamic mechanical tests of the studied nanocomposites are shown in Figures 7 and 8. Typical frequency dependencies of displacement transmissibility are depicted in Figure 7. The obtained results were in excellent agreement with the uniaxial tensile measurements, indicating increased material stiffness based on the f_{R1} peak position shift to the higher excitation frequencies according to equation (4). However, a minor decrease of the latter stiffness was found for low filler concentrations, as indicated by the negligible shift of the f_{R1} to the lower magnitudes (Figure 7a and b). The effect of the inertial mass magnitudes on the frequency dependencies of the displacement transmissibility is demonstrated

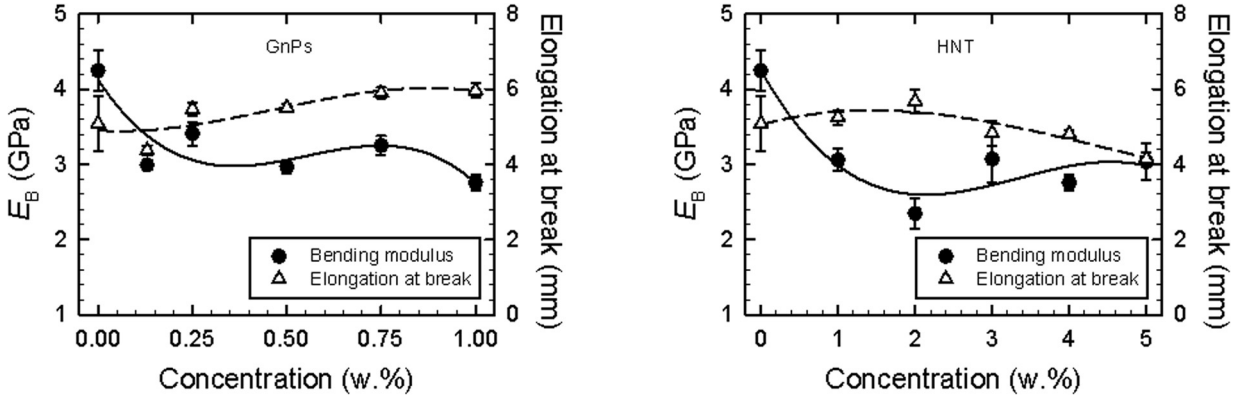

Figure 6: Nanofiller concentration dependencies of the bending modulus and the elongation at break of the studied GnPs and HNT nanocomposites. Applied deformation rate was of 50 mm/min. Continuous line – bending modulus, dashed line – elongation at break.

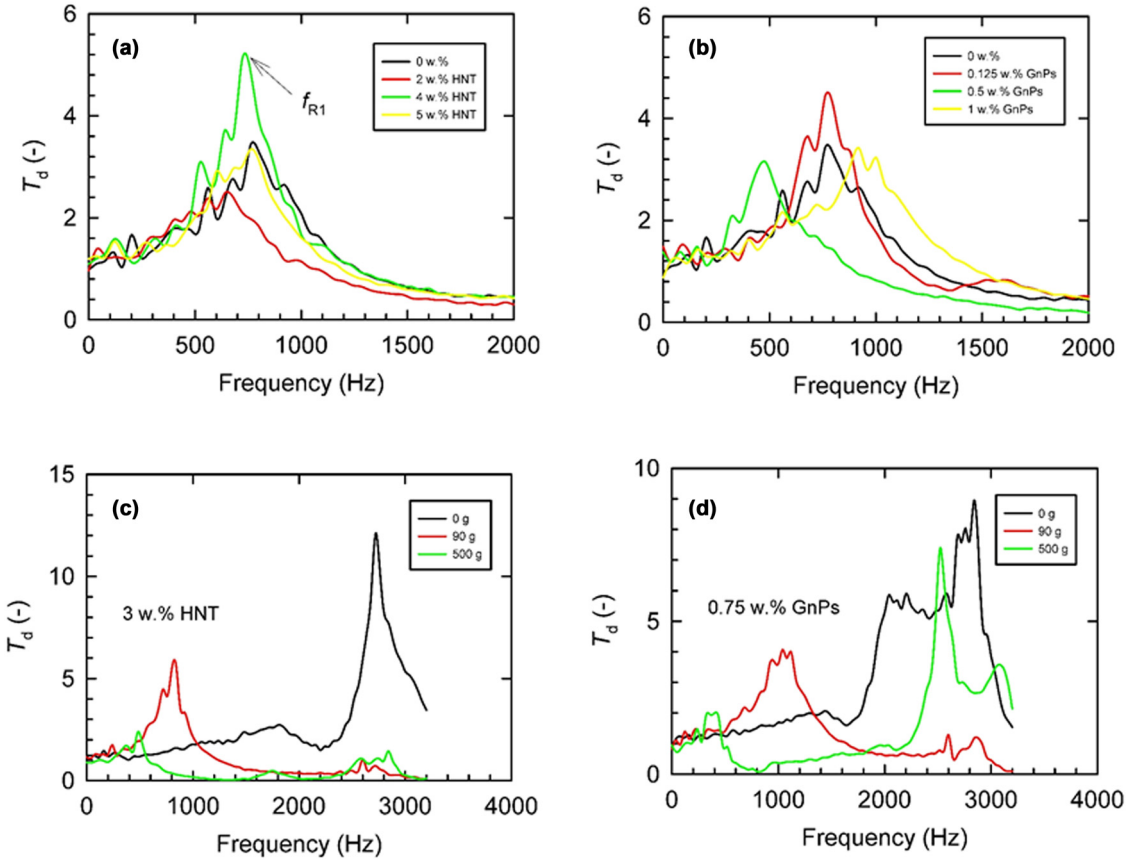

Figure 7: Frequency dependencies of the displacement transmissibility of the tested GnPs and HNT nanocomposites (Inset in a and b: nanofillers concentrations) with applied inertial mass of 90 g (inset in c and d: applied inertial masses).

in Figure 7c and d. It was found that the increasing inertial mass led to the decrease of the first resonance frequency peak position, thereby resulting in the improved materials' mechanical vibration-damping properties [53]. In addition, the obtained increasing f_{R1} with GnP concentration again confirmed materials' increasing stiffness, similar to the case of the previous tensile and fracture toughness measurements (Figures 3 and 4). The latter findings fit very well with the epoxy/GnP nanocomposite results shown in Figure 8, where the linear increase of the f_{R1} with the filler concentration was observed. In contrast, obtained results for the epoxy/HNT nanocomposites exhibited decreased

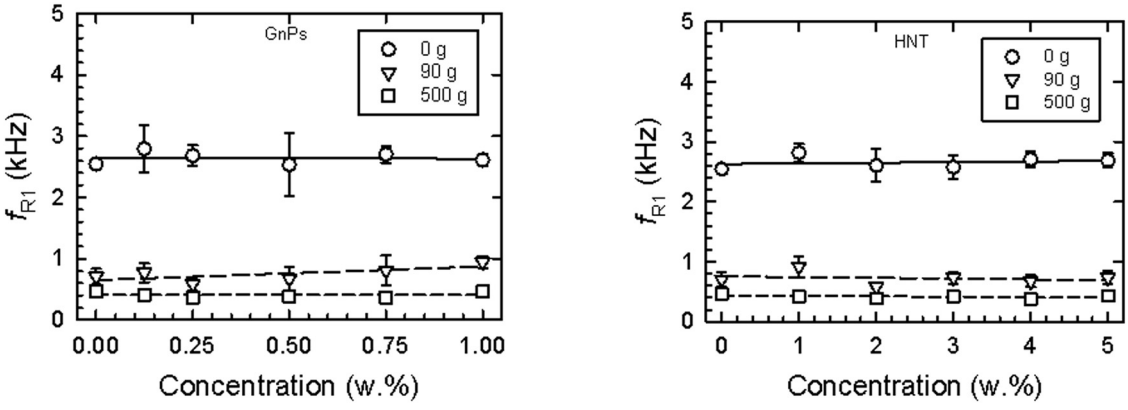

Figure 8: Concentration dependencies of the first resonance frequencies of the studied GnPs and HNT nanocomposites. Inset legend: inertial mass used.

mechanical stiffness as indicated by decreasing f_{R1} with increasing filler concentration for the applied inertial masses.

5 Conclusions

The possibility of elastic–plastic mechanical behavior modulation by means of the application of nanosized GnPs and HNT fillers in the complex epoxy resin-based nanocomposites was confirmed in this study. A complex nonlinear pattern of Young's modulus of elasticity with increasing GnP filler concentration was found. Simultaneously, in the concentration range of 0–1 wt% GnP nanofiller concentration, an increasing ductility of the studied nanocomposites was found, as reflected in the samples' increased elongation at break. This kind of behavior was interpreted by the interparticle gliding effect of the individual GnP nanoparticles dispersed in the complex epoxy resin matrix. A relatively constant trend of Young's modulus of elasticity (approximately of about 2.8 GPa) accompanied by the similar nonlinear pattern of elongation at break (approximately of 0.35 mm) for the studied epoxy/HNT nanocomposites in the concentration range of 1–5 wt% was also found. It was attributed to the hindered local movement of the HNT nanofillers in the matrix during mechanical tests. Fracture mechanical tests confirmed that the fracture toughness obtained at low filler concentrations was higher in the case of the stiff epoxy/HNT nanocomposites compared to the epoxy/GnP nanocomposites due to the GnP filler's gliding-dissipative effect. As obtained by the uniaxial three-point bending tests, the elongation at break measurements confirmed the enhanced plasticity and ductility with increasing GnP filler concentration of the complex epoxy/GnP nanocomposites. This was reflected in the exceeding magnitude of the elongation at break of 6 mm compared to 5.3 mm of the epoxy/HNT nanocomposites (both at 1 wt% nanofiller concentration). A similar effect was also confirmed by micro-hardness tests, where the observed indentation modulus of 3.4 GPa of epoxy/GnP nanocomposites was lower compared to 4.0 GPa of epoxy/HNT nanocomposites (both at 1 wt% nanofiller concentration), thus indicating more dissipative mechanical behavior of the epoxy/GnP nanocomposites. The latter we ascribed to the above-mentioned GnP nanofiller gliding friction. As a novel approach, the nondestructive mechanical vibration damping method of forced oscillations was applied in the low-frequency region of 2–3,200 Hz for the comparison of mechanical properties based on the first resonance frequency peak position. The plastification effect of the epoxy/GnP nanocomposites was confirmed by the lower magnitude of the first resonance frequency peak position of 2.6 kHz compared to the observed magnitude of the f_{R1} of 2.8 kHz for epoxy/HNT nanocomposites (both results obtained at 1 wt% nanofiller concentration and zero inertial mass).

Funding information: This study was supported by the European Regional Development Fund in the Research Centre of Advanced Mechatronic Systems project, project number CZ.02.1.01/0.0/0.0/16_019/0000867. LL and YM would like to express their gratitude for financing this research by the internal grants of Palacky University in Olomouc IGA_PrF_2022_020, IGA_PrF_2023_024 and to Tomas Bata University in Zlin (project nos IGA/FT/2022/005 and IGA/FT/2023/007). Financial support to YM by Fischer scholarship of the Faculty of Science, Palacky University in Olomouc, in the year 2022/2023, is also gratefully acknowledged.

Author contributions: All authors have accepted responsibility for the entire content of this manuscript and approved its submission.

Conflict of interest: The authors state no conflict of interest.

References

[1] Lapcik L, Jindrova P, Lapcikova B, Tamblyn R, Greenwood R, Rowson N. Effect of the talc filler content on the mechanical properties of polypropylene composites. J Appl Polym Sci. 2008 Dec 5;110(5):2742–7.

[2] Bheemappa S, Gurumurthy H. Recent advances in fabrication and characterization of nanofiller filled epoxy nanocomposites. Trends Fabr Polym Polym Compos. 2022;2022:1–40.

[3] Ogbonna VE, Popoola A, Popoola OM, Adeosun SO. A review on the recent advances on improving the properties of epoxy nanocomposites for thermal, mechanical, and tribological applications: challenges and recommendations. Polym Technol Mater. 2022;61(2):176–95.

[4] Krasny I, Lapcik L, Lapcikova B, Greenwood RW, Safarova K, Rowson NA. The effect of low temperature air plasma treatment on physico-chemical properties of kaolinite/polyethylene composites. Compos Part B Eng. 2014 Mar;59:293–9.

[5] Lapcik L, Jindrova P, Lapcikova B. Effect of talc filler content on poly(propylene) composite mechanical properties. Eng Fract. 2009;1:73–80.

[6] Chen X, Li Y, Wang Y, Song D, Zhou Z, Hui D. An approach to effectively improve the interfacial bonding of nano-perfused composites by in situ growth of CNTs. Nanotechnol Rev. 2021;10(1):282–91.

[7] Gouda K, Bhowmik S, Das B. A review on allotropes of carbon and natural filler-reinforced thermomechanical properties of

upgraded epoxy hybrid composite. Rev Adv Mater Sci. 2021 jan;60(1):237–75.
[8] Amin M, Ali M. Polymer nanocomposites for high voltage outdoor insulation applications. Rev Adv Mater Sci. 2015 jun;40(3):276–94.
[9] Lapcik L, Raab M. Materials Science II. Textbook. 2nd edn. Zlin: Tomas Bata University in Zlin; 2004.
[10] Lapcik L', Jancar J, Stasko A, Sáha P. Electron paramagnetic resonance study of free-radical kinetics in ultraviolet-light cured dimethacrylate copolymers. J Mater Sci Mater Med. 1998;9(5):257–62.
[11] Vijayan PP, George JS, Thomas S. The effect of polymeric inclusions and nanofillers on cure kinetics of epoxy resin: A review. Polym Sci Ser A. 2021 Nov;63(6):637–51.
[12] Ouyang CF, Geo Q, Shi YT, Li WT. Effect of CTBN on properties of oxide graphene/epoxy resin composites. Chin Ceram Commun II. 2012;412:393.
[13] Wang FZ, Drzal LT, Qin Y, Huang ZX. Enhancement of fracture toughness, mechanical and thermal properties of rubber/epoxy composites by incorporation of graphene nanoplatelets. Compos Part A Appl Sci Manuf. 2016 August;87:10–22.
[14] Lim YJ, Carolan D, Taylor AC. Simultaneously tough and conductive rubber-graphene-epoxy nanocomposites. J Mater Sci. 2016 Sep;51(18):8631–44.
[15] Xie C, Li Y, Han Y. Fabrication and properties of CTBN/Si3N4/Cyanate ester nanocomposites. Polym Compos. 2016 August;37(8):2522–6.
[16] Konnola R, Joji J, Parameswaranpillai J, Joseph K. Structure and thermo-mechanical properties of CTBN-grafted-GO modified epoxy/DDS composites. RSC Adv. 2015;5(76):61775–86.
[17] Hashim UR, Jumahat A, Jawaid M. Mechanical properties of hybrid graphene nanoplatelet-nanosilica filled unidirectional basalt fibre composites. Nanomaterials. 2021;11(6):1468.
[18] Lapcik L, Manas D, Vasina M, Lapcikova B, Reznicek M, Zadrapa P. High density poly(ethylene)/CaCO3 hollow spheres composites for technical applications. Compos Part B Eng. 2017 Mar 15;113:218–24.
[19] Fiore V, Scalici T, Di Bella G, Valenza A. A review on basalt fibre and its composites. Compos Part B Eng. 2015;74:74–94.
[20] Tarawneh MA, Saraireh SA, Chen RS, Ahmad SH, Al-Tarawni M, Yu LJ, et al. Mechanical reinforcement with enhanced electrical and heat conduction of epoxy resin by polyaniline and graphene nanoplatelets. Nanotechnol Rev. 2020 Jan;9(1):1550–61.
[21] Ma X, Peng C, Zhou D, Wu Z, Li S, Wang J, et al. Synthesis and mechanical properties of the epoxy resin composites filled with sol– gel derived ZrO2 nanoparticles. J Sol Gel Sci Technol. 2018;88(2):442–53.
[22] Sui G, Zhong WH, Liu MC, Wu PH. Enhancing mechanical properties of an epoxy resin using "liquid nano-reinforcements". Mater Sci Eng A. 2009;512(1–2):139–42.
[23] Nath S, Jena H, Sahini D. Analysis of mechanical properties of jute epoxy composite with cenosphere filler. Silicon. 2019;11(2):659–71.
[24] Sim J, Kang Y, Kim BJ, Park YH, Lee YC. Preparation of fly ash/epoxy composites and its effects on mechanical properties. Polymers. 2020;12(1):79.
[25] Kiran MD, Govindaraju HK, Jayaraju T, Kumar N. effect of fillers on mechanical properties of polymer matrix composites. Mater Today Proc. 2018;5(10):22421–4.
[26] Prasob PA, Sasikumar M. Static and dynamic behavior of jute/epoxy composites with ZnO and TiO2 fillers at different temperature conditions. Polym Test. 2018;69:52–62.
[27] Savotchenko S, Kovaleva E, Cherniakov A. The improvement of mechanical properties of repair and construction compositions based on epoxy resin with mineral fillers. J Polym Res. 2022;29(7):1–10.
[28] Zhang HY, Li X, Qian WJ, Zhu JG, Chen BB, Yang J, et al. Characterization of mechanical properties of epoxy/nanohybrid composites by nanoindentation. Nanotechnol Rev. 2020 Jan;9(1):28–40.
[29] Tang L, Wan Y, Yan D, Pei Y, Zhao L, Li Y, et al. The effect of graphene dispersion on the mechanical properties of graphene/epoxy composites. Carbon. 2013;60:16–27.
[30] Ioniţă M, Vlăsceanu GM, Watzlawek AA, Voicu SI, Burns JS, Iovu H. Graphene and functionalized graphene: Extraordinary prospects for nanobiocomposite materials. Compos Part B: Eng. 2017;121:34–57.
[31] Sukur EF, Onal G. Graphene nanoplatelet modified basalt/epoxy multi-scale composites with improved tribological performance. Wear. 2020;460:203481.
[32] Kilic U, Sherif MM, Ozbulut OE. Tensile properties of graphene nanoplatelets/epoxy composites fabricated by various dispersion techniques. Polym Test. 2019;76:181–91.
[33] Wang P, Hsieh T, Chiang C, Shen M. Synergetic effects of mechanical properties on graphene nanoplatelet and multi-walled carbon nanotube hybrids reinforced epoxy/carbon fiber composites. J Nanomater. 2015;2015:1–9.
[34] Mishra BP, Mishra D, Panda P. An experimental investigation of the effects of reinforcement of graphene fillers on mechanical properties of bi-directional glass/epoxy composite. Mater Today Proc. 2020;33:5429–41.
[35] Georgakilas V, Otyepka M, Bourlinos AB, Chandra V, Kim N, Kemp KC, et al. Functionalization of graphene: Covalent and non-covalent approaches, derivatives and applications. Chem Rev. 2012 NOV;112(11):6156–214.
[36] Joussein E, Petit S, Churchman J, Theng B, Righi D, Delvaux B. Halloysite clay minerals - A review. Clay Min. 2005 DEC;40(4):383–426.
[37] Yuan P, Tan D, Annabi-Bergaya F. Properties and applications of halloysite nanotubes: Recent research advances and future prospects. Appl Clay Sci. 2015;112:75–93.
[38] Gaaz TS, Sulong AB, Kadhum AAH, Al-Amiery AA, Nassir MH, Jaaz AH. The impact of halloysite on the thermo-mechanical properties of polymer composites. Molecules. 2017;22(5):838.
[39] Tierrablanca E, Romero-García J, Roman P, Cruz-Silva R. Biomimetic polymerization of aniline using hematin supported on halloysite nanotubes. Appl Catal A: Gen. 2010;381(1–2):267–73.
[40] Kausar A. Review on polymer/halloysite nanotube nanocomposite. Polym Plast Technol Eng. 2018;57(6):548–64.
[41] Kausar A. Polymer coating technology for high performance applications: Fundamentals and advances. J Macromol Sci Part A Pure Appl Chem. 2018;55(5):440–8.
[42] Ghadikolaee MR, Korayem AH, Sharif A, Liu YM. The halloysite nanotube effects on workability, mechanical properties, permeability and microstructure of cementitious mortar. Constr Build Mater. 2021;267:120873.

[43] Hashmi MA. Enhancement of mechanical properties of epoxy/halloysite nanotube (HNT) nanocomposites. SN Appl Sci. 2019;1(4):1–8.
[44] Chen FX, Fan JT, Hui DV, Wang C, Yuan FP, Wu XL. Mechanisms of the improved stiffness of flexible polymers under impact loading. Nanotechnol Rev. 2022 Dec 16;11(1):3281–91.
[45] Srivastava S, Pandey A. Mechanical behavior and thermal stability of ultrasonically synthesized halloysite-epoxy composite. Compos Commun. 2019 Feb;11:39–44.
[46] Alexopoulos ND, Paragkamian Z, Poulin P, Kourkoulis SK. Fracture related mechanical properties of low and high graphene reinforcement of epoxy nanocomposites. Compos Sci Technol. 2017 Sep 29;150:194–204.
[47] Wei JC, Atif R, Vo T, Inam F. Graphene nanoplatelets in epoxy system: Dispersion, reaggregation, and mechanical properties of nanocomposites. J Nanomater. 2015;2015:(3):1–12.
[48] Chatterjee S, Nafezarefi F, Tai NH, Schlagenhauf L, Nuesch FA, Chu B. Size and synergy effects of nanofiller hybrids including graphene nanoplatelets and carbon nanotubes in mechanical properties of epoxy composites. Carbon. 2012 Dec;50(15):5380–6.
[49] Alamri H, Low IM. Microstructural, mechanical, and thermal characteristics of recycled cellulose fiber-halloysite-epoxy hybrid nanocomposites. Polym Compos. 2012 Apr;33(4):589–600.
[50] Oliver WC, Pharr GM. Measurement of hardness and elastic modulus by instrumented indentation: Advances in understanding and refinements to methodology. J Mater Res. 2004 Jan;19(1):3–20.
[51] Manas D, Mizera A, Manas M, Ovsik M, Hylova L, Sehnalek S, et al. Mechanical properties changes of irradiated thermoplastic elastomer. Polymers. 2018 Jan;10(1):87.
[52] Rao SS. Mechanical vibrations. 5th edn. Upper Saddle River, USA: Prentice Hall; 2010.
[53] Lapcik L, Vasina M, Lapcikova B, Stanek M, Ovsik M, Murtaja Y. Study of the material engineering properties of high-density poly(ethylene)/perlite nanocomposite materials. Nanotechnol Rev. 2020 Jan;9(1):1491–9.
[54] Carrella A, Brennan MJ, Waters TP, Lopes V, Jr. Force and displacement transmissibility of a nonlinear isolator with high-static-low-dynamic-stiffness. Int J Mech Sci. 2012;55(1):22–9.
[55] Ab Latif N, Rus AZM. Vibration transmissibility study of high density solid waste biopolymer foam. J Mech Eng Sci. 2014;6:772–81.
[56] Murtaja Y, Lapcik L, Sepetcioglu H, Vlcek J, Lapcikova B, Ovsik M, et al. Enhancement of the mechanical properties of HDPE mineral nanocomposites by filler particles modulation of the matrix plastic/elastic behavior. Nanotechnol Rev. 2022 Jan 5;11(1):312–20.